https://doi.org/10.5194/egusphere-2026-4438
Preprint. Discussion started: 14 September 2026

Contrasting absorption and transport regimes of black and brown carbon across the western, central, and eastern Himalayas

Ju-Lian Shi[1,2,8], Chong-Shu Zhu[1,6*], Yao Qu[1,5], Xiao Wang[1,2], Nan Wang[4], Lu-Yao Wang[1,2], Wen-Ting Dai[1,6], Hong Huang[3#], Jun-Ji Cao[1,7]

[1]*State Key Laboratory of Loess Science, Institute of Earth Environment, Chinese Academy of Sciences, Xi'an 710061, China*

[2]*Xi'an Institute for Innovative Earth Environment Research, Xi'an, 710061, China*

[3]*School of Resources and Environment, Nanchang University, Nanchang 330031, China*

[4]*Xi'an Meteorological Bureau, Xi'an 710016, China*

[5]*University of Chinese Academy of Sciences, Beijing 100049, China*

[6]*National Field Observation and Research Station (Shaanxi) for Ecological and Environment Changes and Integrated Management in the Guanzhong Plain Region, Xi'an 710061, China*

[7]*Institute of Atmospheric Physics, Chinese Academy of Sciences, Beijing 100029, China*

[8]*School of Environmental and Municipal Engineering, Xi'an University of Architecture and Technology, Xi'an 710055, China*

*Corresponding author. Postal address: Institute of Earth Environment, Chinese Academy of Sciences, No. 97 Yan xiang Road, Yan-ta Zone, Xi'an 710061, Shaanxi, China. E-mail: chongshu@ieecas.cn
#Corresponding author. Postal address: School of Resources and Environment, NanChang University, Nanchang 330031, Jiangxi, China. E-mail: honghuang@ncu.edu.cn

https://doi.org/10.5194/egusphere-2026-4438
Preprint. Discussion started: 14 September 2026

Key Points

- Mineral dust, pollution-modified dust, and biomass burning emissions characterized the aerosols in the western, central, and eastern Himalayas, respectively.
- Orographic forcing modulated the spatial distribution of light absorption by carbonaceous aerosols across the Himalayas.
- Primary brown carbon (BrC_{pri}) contributed substantially to light absorption coefficients and aerosol radiative forcing in the central Himalayas.

https://doi.org/10.5194/egusphere-2026-4438
Preprint. Discussion started: 14 September 2026

Abstract

Carbonaceous aerosols strongly influence atmospheric radiative forcing over the Himalayas, yet their spatial variability and transport mechanisms remain poorly constrained. Here we present high-time-resolution measurements of black carbon (BC), primary brown carbon (BrC_{pri}), and secondary brown carbon (BrC_{sec}) at three high-altitude sites across the western (Purang), central (Yadong), and eastern (Zayü) Himalayas during the pre-monsoon period. Distinct spatial gradients in light absorption and biomass burning (BB) tracers (levoglucosan and K^+) reveal pronounced regional heterogeneity. Yadong exhibits the strongest absorption (B_{abs}: 53.1 ± 18.5 Mm^{-1} at 370 nm; 14.2 ± 5.5 Mm^{-1} at 880 nm) and the highest BB influence, indicating a central Himalayan hotspot of polluted aerosol accumulation. BC dominates light absorption across all sites, with its contribution increasing eastward and reaching ~95% at 660 nm in Zayü. In contrast, BrC contributions exhibit strong regional contrasts, with BrC_{pri} dominating absorption in Yadong (8–28%) and BrC_{sec} enhanced in Purang (3–26%). Trajectory analyses indicate that central Himalayan aerosol loading is strongly modulated by orographic uplift and terrain-driven circulation. CALIPSO observations further demonstrate a transition from mineral dust in the west, to pollution-modified dust in the central Himalayas, and biomass-burning aerosols in the east. These results improve our understanding of the sources, transport pathways, and atmospheric transformations of BC, BrC_{pri}, and BrC_{sec} in the Himalayas.

Keywords: *the Himalayas, black carbon, primary brown carbon, secondary brown carbon, radiative forcing*

https://doi.org/10.5194/egusphere-2026-4438
Preprint. Discussion started: 14 September 2026

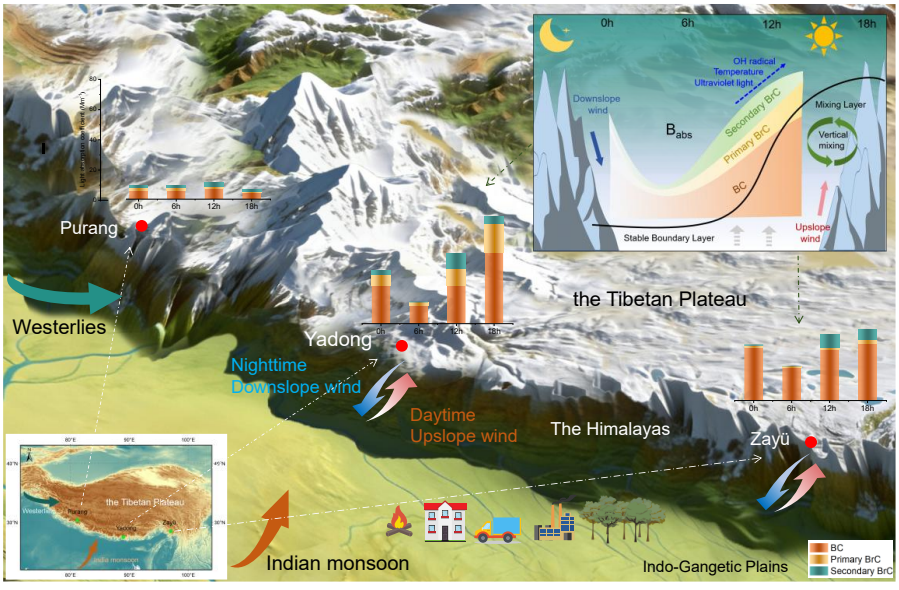

Graph Abstract

https://doi.org/10.5194/egusphere-2026-4438
Preprint. Discussion started: 14 September 2026

1. Introduction

Carbonaceous aerosols influence Earth's radiative balance through the absorption and scattering of solar radiation and by modifying cloud properties (Andreae and Gelencer., 2006; Carslaw et al., 2010; Devaprasad et al., 2024; IPCC, 2013). Black carbon (BC) is a key light-absorbing aerosol, mainly produced by the incomplete combustion of fossil fuels, biomass, and biofuels (Fierce et al., 2020; T. C. Bond et al., 2013; Zhang et al., 2025). In addition to BC, brown carbon (BrC), the light-absorbing fraction of organic aerosol, absorbs radiation across the visible to near-ultraviolet spectrum (approximately 300–700 nm) (Huang et al., 2025; Laskin et al., 2015; Laskin et al., 2025; Rovira et al., 2026). According to its formation pathways, BrC can be classified into primary BrC (BrC_{pri}) and secondary BrC (BrC_{sec}). BrC_{pri} is mainly emitted from biomass burning (BB) and fossil fuel combustion, whereas BrC_{sec} is formed through atmospheric chemical processes (Laskin et al., 2015; Nguyen et al., 2012; Pang et al., 2019). Due to their complex chemical composition and structural diversity, the constituents, optical properties, and radiative effects of BC and BrC require further investigation.

Previous studies have demonstrated that BC contributes significantly to accelerated glacial retreat across the Tibetan Plateau (TP). Moreover, the deposition of BC reduces the albedo of snow and glacier surfaces, thereby influencing regional hydrological cycles (Kopacz et al., 2011; Li et al., 2018; Qian et al., 2011; Qu et al., 2014; Ramachandran et al., 2020; Zhu et al., 2021; Zhu et al., 2024). During the pre-monsoon season, BC concentrations in the Himalayas typically reach their annual maxima, largely due to enhanced BB emissions (Li et al., 2016; Ramachandran et al., 2020; Zhang et al., 2020a). This seasonal enhancement is likely driven by favorable aerosol transport conditions, as Westerlies and the Indian monsoon coincide with elevated aerosol loading in the source regions during the pre-monsoon season (Xu et al., 2020). In addition, atmospheric BrC over South Asia can be lifted to 5,000 m along the southern slopes of the Himalayas (Bonasoni et al., 2010). The observations have further shown that the light absorption by BrC increases with altitude (Zhang et al., 2017).

https://doi.org/10.5194/egusphere-2026-4438
Preprint. Discussion started: 14 September 2026

Previous studies have also shown that pollutant transport over the southern Himalayas is strongly influenced by mountain-valley circulation systems (Hindman and Upadhyay, 2002; Yu et al., 2024; Zhang et al., 2020a).

Due to the harsh environment, the optical properties, transport pathways, and radiative forcing of BC, BrC_{pri}, and BrC_{sec} over the southern Himalayan slopes remain insufficiently characterized, particularly during the pre-monsoon season. This study presents high-time-resolution BC and BrC measurements conducted during three consecutive pre-monsoon seasons (March–May) from 2021 to 2023 at high-altitude sites along the southern slopes of the western, central, and eastern Himalayas. Concurrently, BB tracers were analyzed in total suspended particulate (TSP) samples collected at the same sites. Twenty-four-hour backward and forward trajectories were calculated to investigate aerosol transport pathways. The vertical distribution of aerosols during pollution events was characterized using Cloud-Aerosol Lidar and Infrared Pathfinder Satellite Observations (CALIPSO). Finally, the contributions of BrC_{pri} and BrC_{sec} to direct solar absorption relative to BC were estimated.

2. Methods and Materials

2.1 Sampling and Measurement

The field sampling campaign was conducted at three sites representing the western, central, and eastern Himalayas along the southern Himalayan slope: Purang (30.32° N, 81.17° E, 3,952 m a.s.l.), Yadong (27.52° N, 88.97° E, 3,400 m a.s.l.), and Zayü (28.50° N, 97.02° E, 1900 m a.s.l.) (Table S1). These sites were selected to investigate the spatial variability of carbonaceous aerosols across different sectors of the southern Himalayan slope. Sampling was carried out during the pre-monsoon season (March–May), with field campaigns conducted separately in 2021 at Purang, 2022 at Yadong, and 2023 at Zayü.

A seven-wavelength Aethalometer (model AE33, Magee Scientific Company, Berkeley, CA, USA) was used to measure the aerosol light absorption coefficient (B_{abs}) at wavelengths of 370, 470, 520, 590, 660, 880, and 950 nm (Drinovec et al., 2015).

https://doi.org/10.5194/egusphere-2026-4438
Preprint. Discussion started: 14 September 2026

The spectral B_{abs} was obtained at these wavelengths, and the corresponding BC concentrations were calculated from the measured absorption. The aerosol B_{abs} at wavelength (λ) was determined from the corresponding BC concentration (BC(λ)) and the mass absorption cross-section (MAC(λ)), as described by equation (1) (Drinovec et al., 2015). In this equation, the values of MAC at 370, 470, 520, 590, 660, 880, and 950 nm were 18.47, 14.54, 13.14, 11.58,10.35,7.77, 7.19 m^2g^{-1}, respectively.

$$B_{abs}(\lambda) = BC(\lambda) \times MAC(\lambda) \quad (1)$$

TSP samples were collected on 47 mm Whatman quartz fiber filters (QM/A) using a custom-built high-volume sampler operating at a flow rate of 17 L/min. Sampling was performed continuously over a 7-day period. The concentrations of levoglucosan and potassium (K^+) in the TSP samples were quantified using established analytical methods (see Text S1 for details).

2.2 Data analysis methods

The B_{abs} of BC, BrC_{pri}, and BrC_{sec} can be derived according to the assumption that BrC absorption is zero at λ = 880 nm (Bahadur et al., 2012; Kirchstetter et al., 2012; Lu et al., 2015; Saleh et al., 2014). The B_{abs}(BC) at each wavelength was calculated by extrapolating the absorption at 880 nm using a absorption Ångström exponent (AAE_{BC}) of 1.1 (Qu et al., 2022). BrC absorption at each wavelength was then estimated as the difference between the measured total aerosol absorption and the corresponding BC absorption. As BC is generated from combustion, a BC-tracer method was utilized to estimate the primary B_{abs} (λ). The minimum R-squared method (MRS) was applied to derive the light absorption of BrC_{sec} across the full measurement wavelength range. This approach was adapted from the commonly employed BC-tracer technique originally developed for secondary organic carbon (SOC) quantification (Srivastava et al., 2018; Wang et al., 2019). Based on the negligible dust contribution, the MRS can separate $B_{abs}(BrC_{sec})$ versus the light absorption by BrC_{pri} ($B_{abs}(BrC_{pri})$ (Wang et al., 2019).

$$B_{abs}(BrC_{sec})(\lambda) = B_{abs}(\lambda) - \left(\frac{B_{abs}(\lambda)}{BC}\right)_{pri} \times [BC] \quad (2)$$

https://doi.org/10.5194/egusphere-2026-4438
Preprint. Discussion started: 14 September 2026

[BC] represents the ambient BC concentration (μg m^{-3}). The parameter $\left(\frac{B_{abs}(\lambda)}{BC}\right)_{pri}$ denotes the ratio between the B_{abs} (λ) and the BC mass concentration from primary emissions, with units of m^2 g^{-1}. $B_{abs}(BrC_{pri})$ (λ) is derived via the equation provided below:

$$B_{abs}(BrC_{pri})(\lambda) = B_{abs}(BrC)(\lambda) - B_{abs}(BrC_{sec})(\lambda) \quad (3)$$

The total BrC absorption coefficient ($B_{abs}(BrC)(\lambda)$) (Mm^{-1}) is derived by removing the BC contribution from the total absorption measured at $B_{abs}(\lambda)$. This calculation rests on the premise that BC constitutes the sole light-absorbing species at the 880 nm wavelength. A detailed description of the methodology is provided in Wang et al., (2019).

The direct solar absorption contributions of BrC_{pri} and BrC_{sec} relative to BC at the Purang, Yadong, and Zayü sampling sites were derived using a previously validated protocol described in previous studies (Huang et al., 2018; Kirillova et al., 2014). The light absorption by the species x (BrC_{pri} and BrC_{sec}, or BC) is computed in accordance with the Beer-Lambert's law, as shown in the equation below:

$$\frac{I_0 - I}{I_0}(\lambda) = 1 - e^{-b_{ap,x,\lambda} \cdot h_{ABL}} \quad (4)$$

In this equation, the atmospheric boundary layer height (h_{ABL}) is assumed to be 1000 m. For a given wavelength (λ) and absorbing aerosol component (x), $b_{ap,x,\lambda}$ denotes the component-specific aerosol absorption coefficient, representing either the BC absorption coefficient or the BrC absorption coefficient for BC and BrC, respectively. The relative contribution of BrC to solar radiation absorption compared with BC is then quantified using the following equation.

$$f = \frac{\int I_0(\lambda)\left\{1 - e^{-b_{ap,BrC(Primary/Secondary),\lambda} \cdot h_{ABL}}\right\} d\lambda}{\int I_0(\lambda)\left\{1 - e^{-b_{ap,BC,\lambda} \cdot h_{ABL}}\right\} d\lambda} \quad (5)$$

where $I_0(\lambda)$ represents the clear sky Air Mass 1 Global Horizontal solar irradiance at wavelength λ (Levinson et al., 2010). The fraction *f* is derived via numerical integration

https://doi.org/10.5194/egusphere-2026-4438
Preprint. Discussion started: 14 September 2026

of the above expression across the entire sampling campaign, applied separately to three distinct wavelength intervals spanning 300–400, 300–700, and 300–950 nm, respectively (Huang et al., 2018).

2.3 Application of software models

The Hybrid Single-Particle Lagrangian Integrated Trajectory (HYSPLIT) model was used to assess air mass transport pathways to the sampling site, which was developed by the National Oceanic and Atmospheric Administration's Air Resources Laboratory (NOAA/ARL) (Draxler and Rolph, 2012). Using meteorological data from the Global Data Assimilation System (GDAS, ftp://arlftp.arlhq.noaa.gov/pub/archives/gdas1/) with a spatial resolution of 1°×1°, twenty-four-hour backward and forward trajectories were produced on a six-hourly schedule, all terminating at 500 meters above ground level. To identify dominant air mass transport pathways, trajectory clustering analysis was performed by grouping trajectories according to their spatial similarity. The Euclidean distance between corresponding trajectory coordinates was used as the similarity metric.

The CALIPSO satellite, launched in April 2006, is a joint NASA–CNES mission equipped with the Cloud-Aerosol Lidar with Orthogonal Polarization (CALIOP) as its primary instrument. CALIOP is a dual-wavelength polarization-sensitive lidar operating at 532 and 1064 nm (Hunt et al., 2009; Winker et al., 2007; Winker et al., 2009). The sensor provides global vertical distribution information of aerosols and clouds, making it particularly suitable for aerosol studies in regions with sparse ground-based observations, such as the polar regions and the TP (Liu et al., 2008). This study utilizes two CALIPSO Level 2 products to obtain vertical distribution information of aerosols and clouds in the sites, namely the Aerosol Profile and the Vertical Feature Mask, version V4.51, obtained from the NASA Langley Research Center Atmospheric Science Data Center (https://asdc.larc.nasa.gov/). Detailed information is provided in the supplementary material (Text S2).

https://doi.org/10.5194/egusphere-2026-4438
Preprint. Discussion started: 14 September 2026

3. Results and discussion

3.1 Enhanced Carbonaceous Aerosol Light Absorption in the Central Himalayas

Carbonaceous aerosol light absorption coefficients at 370 nm ($B_{abs,370}$) and 880 nm ($B_{abs,880}$) were simultaneously measured at three sites along the southern slopes of the Himalayas (Figure 1). At all sites, $B_{abs,370}$ consistently exceeded $B_{abs,880}$, suggesting a contribution from BrC in addition to BC. During the pre-monsoon season, the highest absorption coefficients were observed at Yadong, reaching 53.1 ± 18.5 Mm^{-1} at 370 nm and 14.2 ± 5.5 Mm^{-1} at 880 nm. The $B_{abs,370}$ value was 2.8 times greater than $B_{abs,880}$, indicating enhanced absorption by BrC in the near-ultraviolet wavelength range. In Zayü, the average absorption coefficients during the pre-monsoon were 31.5 ± 14.9 Mm^{-1} at 370 nm and 13.1 ± 6.1 Mm^{-1} at 880 nm. In contrast, the lowest average absorption coefficients were observed in Purang, with values of 7.5 ± 6.5 Mm^{-1} at 370 nm and 1.9 ± 1.6 Mm^{-1} at 880 nm. These results suggest that carbonaceous aerosols exhibited substantially stronger light absorption in the central Himalayas compared with those in the eastern and western Himalayan regions.

Previous studies have suggested that BB emissions from northern India can enhance shortwave aerosol absorption above clouds over the central Himalayas during spring (Kumar et al., 2011). The weekly averaged levoglucosan concentrations ranged from 17.8 to 1688.9 ng m^{-3} at Purang, 280.8 to 2041.7 ng m^{-3} at Yadong, and 1.0 to 4.6 ng m^{-3} at Zayü. The seasonal mean levoglucosan concentrations were 518.5 ± 567.6 ng m^{-3} at Purang, 812.0 ± 457.8 ng m^{-3} at Yadong, and 2.0 ± 1.3 ng m^{-3} at Zayü. Compared with previous studies, lower annual mean levoglucosan concentrations were reported for Ngari (232.8 ± 149.5 ng m^{-3}), Qinghai Lake (65.5 ± 39.6 ng m^{-3}), and Beiluhe (0.8 ± 0.7 ng m^{-3}) (Zhu et al., 2022b), suggesting a stronger influence of BB emissions along the southern slopes of the Himalayas than in other regions of the TP.

The seasonal mean K^+ concentrations were 425.3 ± 289.0 ng m^{-3}, 240.7 ± 150.5 ng m^{-3}, and 151.4 ± 89.1 ng m^{-3} at Purang, Yadong, and Zayü, respectively. K^+ exhibited a wider concentration range in Purang (88.1–945.4 ng m^{-3}) than in Yadong (66.5–536.8 ng m^{-3}) and Zayü (22.3–313.3 ng m^{-3}). Overall, the two BB tracers showed the lowest

https://doi.org/10.5194/egusphere-2026-4438
Preprint. Discussion started: 14 September 2026

concentrations in the eastern region, whereas substantially elevated concentrations were observed in the central and western regions. The enhanced optical absorption observed in the central Himalayas was likely associated, at least partly, with BB influences, as evidenced by elevated concentrations of levoglucosan and K^+ at sites along the southern Himalayan slopes.

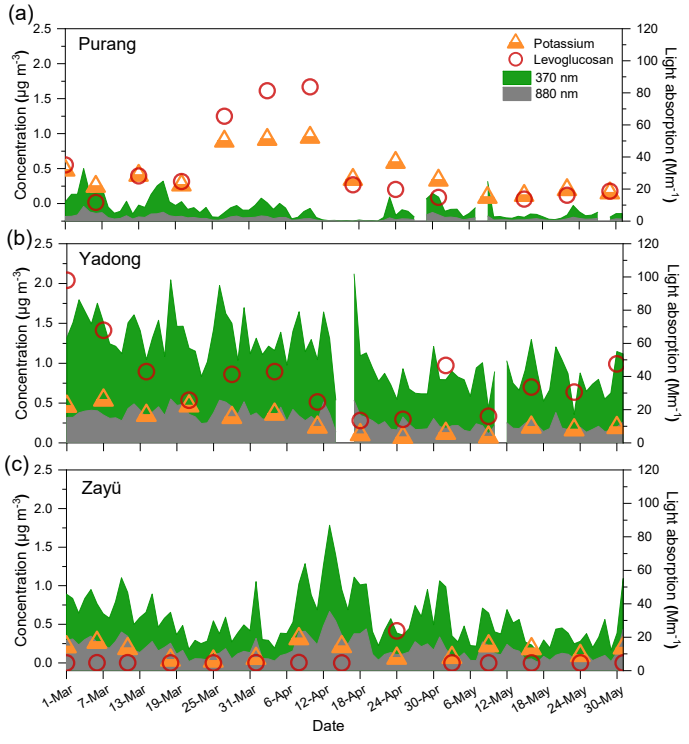

Figure 1. Variations of K^+, levoglucosan, and light absorption coefficient (370 nm and 880 nm) in Purang (a), Yadong (b), and Zayü (c), respectively.

3.2 Primary Emissions Dominate Carbonaceous Aerosol Absorption

Figure 2 presents the temporal variations in $B_{abs}(BC)_{370}$, $B_{abs}(BrC_{pri})_{370}$, and $B_{abs}(BrC_{sec})_{370}$, together with temperature, relative humidity (RH), and wind speed at Purang, Yadong, and Zayü. Among the three absorbing components, BC consistently exhibited the highest absorption at 370 nm. Mean $B_{abs}(BC)_{370}$ values were 5.6 ± 4.0 Mm^{-1} at Purang, 47.7 ± 17.0 Mm^{-1} at Yadong, and 36.4 ± 16.9 Mm^{-1} at Zayü, with daily values ranging from 0.1–22.2, 14.0–95.4, and 12.3–94.3 Mm^{-1}, respectively.

https://doi.org/10.5194/egusphere-2026-4438
Preprint. Discussion started: 14 September 2026

The highest mean $B_{abs}(BrC_{pri})_{370}$ was also observed at Yadong (21.9 ± 6.6 Mm^{-1}), which was approximately 13.3 and 20.1 times higher than those at Purang (1.6 ± 1.1 Mm^{-1}) and Zayü (1.1 ± 0.7 Mm^{-1}), respectively. Daily $B_{abs}(BrC_{sec})_{370}$ ranged from 0.1 to 27.2 Mm^{-1} at Purang, 0.1 to 32.8 Mm^{-1} at Yadong, and 0.4 to 58.0 Mm^{-1} at Zayü. Although mean $B_{abs}(BrC_{sec})_{370}$ in Yadong (10.0 ± 7.1 Mm^{-1}) was lower than $B_{abs}(BC)_{370}$ and $B_{abs}(BrC_{pri})_{370}$, it remained the highest among the three sites. Mean $B_{abs}(BrC_{sec})_{370}$ values were 5.7 ± 9.4 Mm^{-1} and 2.8 ± 3.6 Mm^{-1} at Zayü and Purang, respectively, both exceeding the corresponding $B_{abs}(BrC_{pri})_{370}$ values, suggesting a stronger contribution of BrC_{sec} to light absorption at these sites.

Overall, $B_{abs}(BC)_{370}$, $B_{abs}(BrC_{pri})_{370}$, and $B_{abs}(BrC_{sec})_{370}$ all reached their highest absolute levels in the central Himalayas, indicating a stronger influence of primary emissions in this region. In contrast, BrC_{sec} contributed more to light absorption than BrC_{pri} in the eastern and western Himalayas.

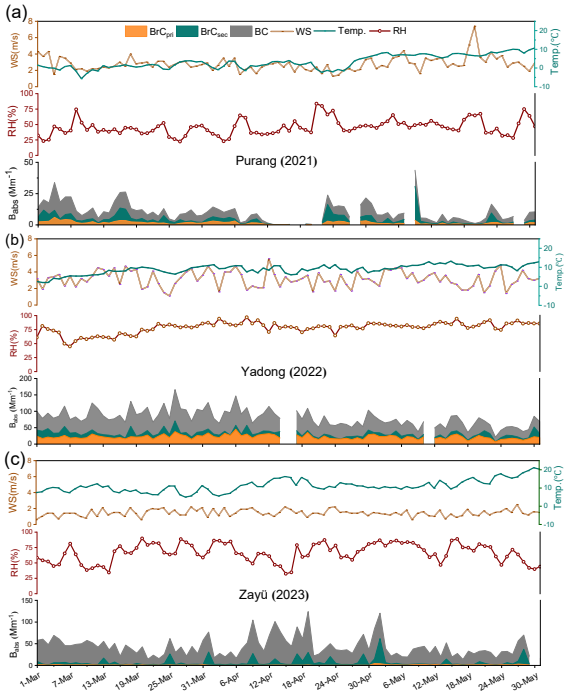

Figure 2. Light absorption of the BC, BrC_{pri}, and BrC_{sec} at 370 nm and associated meteorological parameters (wind speed, relative humidity, and temperature) at Purang (a), Yadong (b), and Zayü (c), respectively.

https://doi.org/10.5194/egusphere-2026-4438
Preprint. Discussion started: 14 September 2026

3.3 Spatial Variations in BC, BrC_{pri}, and BrC_{sec} Contributions

Figure 3 (I) presents the mean $B_{abs}(BC)$, $B_{abs}(BrC_{pri})$, and $B_{abs}(BrC_{sec})$, together with their contributions to total light absorption across wavelengths from 370 to 660 nm. $B_{abs}(BC)$, $B_{abs}(BrC_{pri})$, and $B_{abs}(BrC_{sec})$ all decreased with increasing wavelength. The highest $B_{abs,370}$ was observed at Yadong (79.6 ± 25.5 Mm^{-1}), approximately 1.8 and 8 times higher than those at Zayü and Purang, respectively.

BC was the dominant light-absorbing component across the measured wavelength range at all three sites, consistent with previous observations (Ramachandran et al., 2020). Its contribution increased from the western to the eastern Himalayas. At 370 nm, BC accounted for 56%, 60%, and 84% of total absorption in Purang, Yadong, and Zayü, respectively. The highest BC contribution was observed in Zayü at 660 nm (95%).

The contribution of BrC_{pri} to total absorption was highest at Yadong and exceeded that of BrC_{sec} throughout the measured wavelength range. At Yadong, BrC_{pri} accounted for 28%, 18%, 12%, 10%, and 8% of total absorption at 370, 470, 520, 590, and 660 nm, respectively. In contrast, the lowest BrC_{pri} contribution was observed at Zayü (4%).

The contribution of BrC_{sec} to total absorption decreased from the western to the eastern Himalayas. The highest BrC_{sec} contributions were observed at Purang, reaching 26%, 13%, 9%, 6%, and 3% at 370 nm, 470 nm, 520 nm, 590 nm, and 660 nm, respectively. As shown in Figure 3 (II), the mean daily $B_{abs}(BrC_{sec})/B_{abs}(BrC)$ ratios at 370 nm were 0.56, 0.29, and 0.50 for Purang, Yadong, and Zayü, respectively. These results indicate that BrC_{sec} contributed a larger fraction of total BrC absorption in the western and eastern Himalayas, whereas BrC_{pri} made a relatively greater contribution in the central Himalayas.

https://doi.org/10.5194/egusphere-2026-4438
Preprint. Discussion started: 14 September 2026

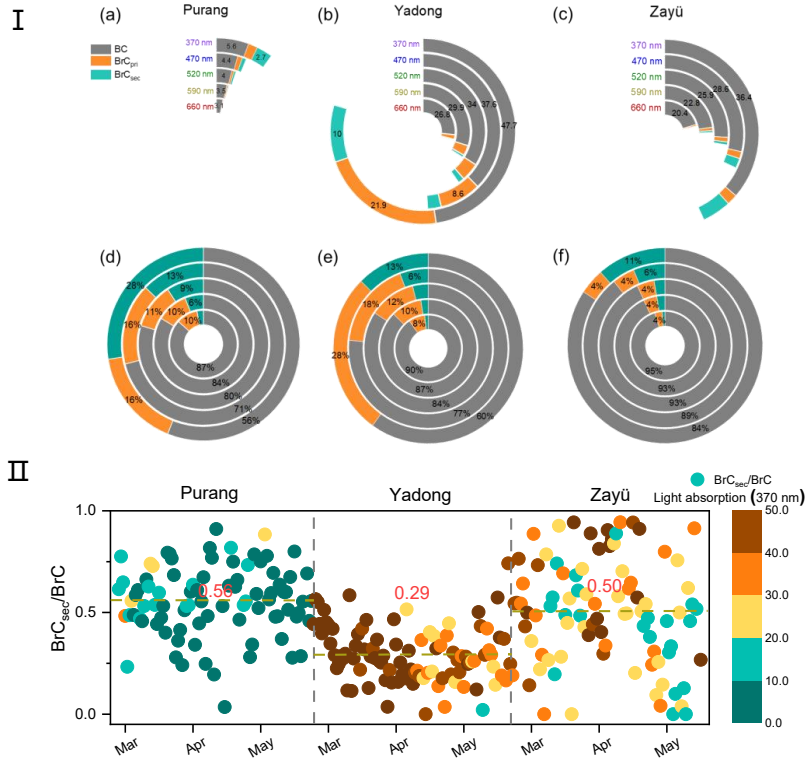

Figure 3. Relative contributions of BC, BrC_{pri}, and BrC_{sec} to B_{abs} (a-c), and wavelength-dependent absolute light absorption of BC, BrC_{pri}, and BrC_{sec} for Purang, Yadong, and Zayü (d-f), respectively (I). Ratios of BrC_{sec}/BrC at 370 nm for Purang, Yadong, and Zayü, respectively; the color of the points represents total light absorption at 370 nm (II).

3.4 Spectral Dependence of Aerosol Absorption and Implications for BrC Sources

The absorption Ångström exponent (AAE) is widely used to characterize the wavelength dependence of aerosol light absorption and to infer the relative contributions of different light-absorbing aerosol components. As shown in Table 1, the mean AAE values (370–950 nm) were 1.77, 1.71, and 1.22 at Purang, Yadong, and Zayü, respectively, exceeding those reported for Lhasa (1.04) and Lulang (1.18) during the postmonsoon season (Zhu et al., 2017). The relatively higher AAE values at Purang and Yadong suggest a greater influence of BB-related BrC, whereas the lower AAE at Zayü is more consistent with absorption dominated by BC from fossil-fuel combustion (Kirchstetter et al., 2004).

At all three sites, AAE values for BrC_{sec} exceeded those for BrC_{pri}. This likely reflects

https://doi.org/10.5194/egusphere-2026-4438
Preprint. Discussion started: 14 September 2026

the stronger wavelength dependence of absorption by BrC_{sec} chromophores, which preferentially absorb radiation at shorter wavelengths. The elevated AAE values of BrC (4.3) and BrC_{pri} (4.0) at Yadong may be associated with the enhanced contribution of BrC_{pri} to total aerosol absorption. The AAE values of BrC_{sec} followed the order Yadong (5.3) > Purang (5.2) > Zayü (4.5). These results further suggest that BrC_{sec} also represents a non-negligible contributor to carbonaceous aerosol light absorption in the Himalayas.

3.5 Orographic Control of Aerosol Transport across the Himalayas

Figure 4 presents 24-h backward and forward air-mass trajectories at Purang, Yadong, and Zayü during the pre-monsoon period. At Purang and Zayü, >94.6% of backward trajectories originated from low-altitude regions, and >98.9% of forward trajectories entered the TP, indicating efficient cross-Himalayan transport through canyon topography. In contrast, Yadong showed mixed transport pathways, with the north–south valley dominating (61.9–85.9%), while plateau and transverse valley contributions were smaller. Most forward trajectories (69.6–98.9%) entered the plateau, while a fraction recirculated within adjacent valleys (see Table S2 for details). These results indicate that aerosol transport in the central Himalayas is strongly modulated by complex terrain and valley circulations, which enhance cross-Himalayan exchange (Yu et al., 2024; Zhang et al., 2020a).

$B_{abs}(BC)$, $B_{abs}(BrC_{pri})$, and $B_{abs}(BrC_{sec})$ exhibited pronounced diurnal cycles with two daytime peaks and a nighttime minimum (Figure 4 I). Morning peaks likely reflect nocturnal accumulation in elevated valley layers followed by daytime upslope transport (Sellegri et al., 2010). At Yadong, $B_{abs}(BC)$ and $B_{abs}(BrC_{pri})$ peaked at 18 h, consistent with primary emissions. $B_{abs}(BrC_{sec})$ peaked around noon at all sites, indicating enhanced daytime secondary formation. In Zayü, BrC_{sec} contributed 74.5–83.9% of BrC absorption during daytime, suggesting a strong influence of secondary formation and regional transport. Satellite observations further show widespread pre-monsoon aerosol loading over South Asia, with westerly flow and local valley circulations jointly enhancing aerosol accumulation along the southern Himalayas (Figure S1, Text S3).

https://doi.org/10.5194/egusphere-2026-4438
Preprint. Discussion started: 14 September 2026

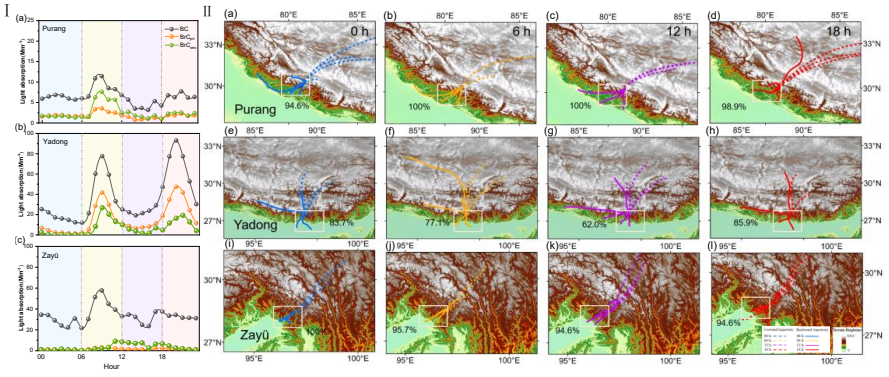

Figure 4. Diurnal patterns of 6-h integrated BC, BrC_{pri}, and BrC_{sec} at 370 nm (I (a-c)). 24-h air-mass trajectory cluster analysis for Purang (a), Yadong (b), and Zayü (c), respectively (II (a-l)).

Fire counts (https://firms.modaps.eosdis.nasa.gov/) indicate low local emissions over the TP during the pre-monsoon period (Figure 5 a-c), while active combustion sources are mainly distributed in South and Southeast Asia. The PSCF was calculated using $B_{abs}(BC)_{370}$, $B_{abs}(BrC_{pri})_{370}$, and 72-h back trajectories at 00, 06, 12, and 18 local standard time (Text S4). Cluster analysis of backward trajectories identified dominant transport pathways for Purang (C1–C4), Yadong (C1–C5), and Zayü (C1–C4) (Table S3).

At Purang, air masses from India (C1, C2) dominated the transport pathways (48 and 38%), with C2 showing the highest $B_{abs}(BC)_{370}$ (7.6 Mm^{-1}) and $B_{abs}(BrC_{pri})_{370}$ (2.2 Mm^{-1}), indicating polluted air mass influence. At Yadong, the dominant cluster (C1, 65%) also originated from India, with $B_{abs}(BC)_{370}$ and $B_{abs}(BrC_{pri})_{370}$ reaching 47.4 and 21.6 Mm^{-1}, respectively. Air masses from the southwestern TP (C2, 16%) were also observed. At Zayü, air masses were mainly transported along the Chayu River valley from Myanmar, Bangladesh, and India. PSCF analysis showed spatial patterns consistent with regional fire activity, highlighting the potential influence of BB and fossil-fuel combustion sources in South and Southeast Asia, while suggesting a weaker contribution from local emissions. Overall, aerosol distributions over the southern Himalayas appear to be shaped by the combined effects of regional transport and topography-driven circulation. (Zhang et al., 2020a).

https://doi.org/10.5194/egusphere-2026-4438
Preprint. Discussion started: 14 September 2026

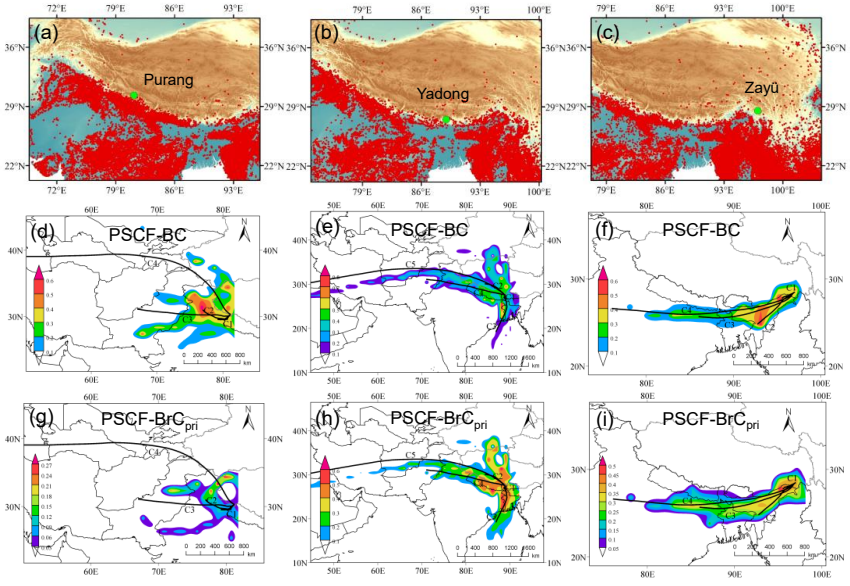

Figure 5. Seasonal distributions of fire hot spots from the Terra and Aqua satellites during the sampling period (a-c). The 72-h backward air-mass trajectory clusters and potential source regions of B_{abs}(BC) and B_{abs}(BrC_{pri}) in Purang, Yadong, and Zayü, respectively (d-g).

3.6 Contrasting Aerosol Vertical Structures across the Southern Himalayas

Figure 6 presents CALIPSO profiles during representative aerosol pollution episodes at the three sites, which corresponded to consistently elevated B_{abs} (Table S4). Marked differences were observed in vertical aerosol profiles across the western, central, and eastern Himalayas during the pre-monsoon season. In the western Himalayas, the aerosol layer followed the terrain with a thickness of 2–3 km. Extinction (2 km^{-1}) and backscatter (4×10^{-3} km^{-1} sr^{-1}) showed a slight decrease, while volume depolarization ratio (VDR) and color ratio (CR) decreased from 0.4 to 0.1 and from 1.0 to 0.5, respectively, suggesting the presence of mixed dust and polluted aerosol layers associated with anthropogenic influence and long-range transport. This is consistent with enhanced BrC_{sec} absorption at Purang.

In the central Himalayas, a ~4 km thick dust layer persisted above 5 km altitude, with extinction (~0.04 km^{-1}) and backscatter (~7×10^{-4} km^{-1} sr^{-1}) decreasing with height. In the lower troposphere (0–4 km) over northern India and Bhutan, higher extinction (1.6 km^{-1}) and backscatter (3×10^{-3} km^{-1} sr^{-1}) were observed, together with low VDR (~0.1)

https://doi.org/10.5194/egusphere-2026-4438
Preprint. Discussion started: 14 September 2026

and moderate CR (~0.5), indicating polluted dust mixed with smoke. This likely contributed to the highest B_{abs} observed at Yadong.

In the eastern Himalayas, extinction (0.075 km^{-1}) and backscatter (1 × 10^{-3} km^{-1} sr^{-1}) were lower along air-mass pathways originating from Myanmar and northern India. The combination of elevated CR (~0.5) and low VDR (~0.1) suggests diluted polluted dust, while elevated BC absorption indicates long-range transport of BB aerosols influencing Zayü.

Overall, the southern Himalayas are influenced by multiple aerosol transport regimes, including dust-dominated, pollution-modified dust, and BB-influenced aerosols in the western, central, and eastern regions, respectively. Compared with Arctic and Antarctic regions, which are generally characterized by relatively pristine marine and mineral dust-dominated aerosol (Yang et al., 2021), the southern Himalayas exhibit more complex aerosol mixtures influenced by mineral dust, BB emissions, and anthropogenic pollution.

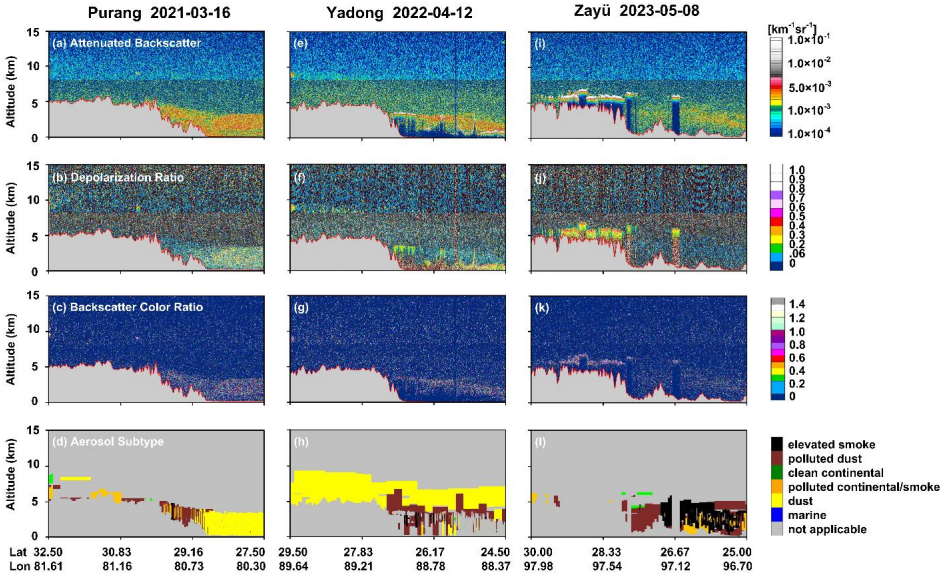

Figure 6. CALIPSO overpass aerosol vertical profile, including attenuated backscatter (a,e,i), depolarization ratio (b,f,j), backscatter color ratio (c,g,k), and aerosol subtype (d,h,l) over the Himalayan on representative aerosol pollution episodes:16 March 2021 (Purang), 12 April 2022 (Yadong), and 8 May 2023 (Zayü), respectively.

https://doi.org/10.5194/egusphere-2026-4438
Preprint. Discussion started: 14 September 2026

3.7 Spatial Variability in the Radiative Forcing of BrC

Radiative forcing contributions of BrC_{pri} and BrC_{sec} relative to BC were evaluated at three sites during the pre-monsoon period (Table 1). In the UV range (300–400 nm), relative radiative forcing contributions of BrC_{pri}/BC were 34.3% (Purang), 54.1% (Yadong), and 5.3% (Zayü), respectively. These values were higher than those reported for the northeastern TP (Qinghai Lake, 16.7%), central TP (Beiluhe, 2.4%), and southwestern TP (Ngari,13.2%) (Zhu et al., 2021).

The highest radiative forcing contributions of BrC_{sec}/BC were observed at Purang (55.7%), followed by Yadong (25.7%) and Zayü (15.5%), indicating an important contribution of BrC_{sec} to aerosol radiative absorption, particularly in the western Himalayas. Over the full solar spectrum (300–950 nm), BrC_{pri}/BC contributions decreased to 19.0%, 21.3%, and 4.3% at Purang, Yadong, and Zayü, respectively. Nevertheless, the relative radiative forcings of BrC_{pri}/BC (300–950 nm) exceeded those of BrC_{sec}/BC in Purang (16.2%) and Yadong (7.9%). Overall, these results suggest a stronger radiative influence of BrC_{sec} in the western Himalayas, whereas BrC_{pri} contributes relatively more to aerosol absorption in the central Himalayas.

Table 1. Aerosol light absorption coefficients and Ångström absorption exponents (AAE) of BC, $BrC_{pri,}$ and $BrC_{sec,}$ and the relative direct solar absorption of BrC_{pri} and BrC_{sec} compared with BC at three sites.

	Parameters	Purang	Yadong	Zayü
Seasonal Light absorption coefficient (Mm^{-1})	$B_{abs}(BC)_{370}$	5.6±4.0	47.7±16.9	36.4±17.0
	$B_{abs}(BrC)_{370}$	4.4±4.4	31.9±11.0	6.8±9.6
	$B_{abs}(BrC_{pri})_{370}$	1.6±1.1	21.9±6.6	1.1±0.7
	$B_{abs}(BrC_{sec})_{370}$	2.8±3.6	10.0±7.1	5.7±9.4
Absorption Ångstrom Exponent	$AAE_{370/950}$	1.77	1.71	1.22
	$AAE_{BrC\ (330/660)}$	3.96	4.40	3.18
	$AAE_{BrCpri\ (330/660)}$	2.70	4.07	1.33
	$AAE_{BrCsec(330/660)}$	5.22	5.30	4.50
BrC_{pri}/BC(%)	$f_{300\text{-}400\ nm}$	34.3±5.9%	54.1±12.1%	5.3±2.6%

https://doi.org/10.5194/egusphere-2026-4438
Preprint. Discussion started: 14 September 2026

BrC_{sec}/BC(%)	$f_{300\text{-}700nm}$	21.6±3.3%	25.6±4.3%	4.4±1.2%
	$f_{300\text{-}950nm}$	19.0±2.9%	21.3±3.5%	4.3±0.9%
	$f_{300\text{-}400\ nm}$	55.7±12.7%	25.7±5.9%	15.5±5.8%
	$f_{300\text{-}700nm}$	20.0±5.0%	9.7±1.9%	6.2±2.6%
	$f_{300\text{-}950nm}$	16.2±4.1%	7.9±1.5%	5.1±2.1%

4. Conclusion

Light absorption by carbonaceous aerosols, including BC, BrC_{pri}, and BrC_{sec}, together with BB tracers (levoglucosan and K^+), was investigated at three high-altitude Himalayan sites during the pre-monsoon period. The results showed that the central site exhibited the highest B_{abs}, with mean values of 53.1 ± 18.5 Mm^{-1} at 370 nm and 14.2 ± 5.5 Mm^{-1} at 880 nm, and also showed elevated concentrations of BB tracers. The observed B_{abs} and levoglucosan concentrations were higher than those reported for the northeastern, central, and southwestern TP (Zhu et al., 2021; Zhu et al., 2022b), with the elevated levoglucosan concentrations suggesting a stronger influence of BB emissions along the southern slopes of the Himalayas. BC was the dominant light-absorbing component across the investigated wavelength range, consistent with observations from other high-altitude regions (Ramachandran et al., 2020; Zhu et al., 2022a). The BC contribution to total light absorption increased from the western to the eastern Himalayas, reaching ~95% at 660 nm at Zayü, which was higher than values reported for most other regions (Zhu et al., 2021). Across the investigated wavelengths, BrC_{pri} and BrC_{sec} contributed 8–28% and 3–26% of total light absorption, respectively, with the highest BrC_{pri} and BrC_{sec} contributions observed at the central and western sites, respectively. Additionally, the central Himalayan site exhibited a stronger BrC_{pri} contribution to solar radiation absorption, in contrast to other sites in the TP and Himalayan regions where BrC_{sec} was reported to make a greater contribution to radiative forcing (Zhu et al., 2021). Together with the elevated BB tracer concentrations,

https://doi.org/10.5194/egusphere-2026-4438
Preprint. Discussion started: 14 September 2026

the enhanced BrC_{pri} contribution suggests a stronger influence of primary combustion emissions, particularly BB emissions, in the central Himalayas.

Previous studies have shown that pollutant transport over the southern Himalayas is strongly influenced by mountain-valley circulation systems (Yu et al., 2024; Zhang et al., 2020a). Our results indicate that transboundary transport from South and Southeast Asia is strongly modulated by the complex Himalayan topography and terrain-induced atmospheric circulation, with particularly pronounced influences in the central Himalayan region. Importantly, consideration of the vertical distribution of aerosols provides additional insight into their regional transport and source characteristics. CALIPSO observations further reveal distinct vertical aerosol profiles, with mineral dust, pollution-modified dust, and BB-related aerosols predominating over the western, central, and eastern Himalayas, respectively. Together, these results highlight pronounced spatial heterogeneity in carbonaceous aerosol characteristics, transport pathways, and associated radiative impacts over the southern Himalayas. These findings further improve our understanding of the vertical distribution, sources, and atmospheric transformation of carbonaceous aerosols over the Himalayas.

However, it should be noted that quantitative estimations of BrC absorption based on spectral apportionment commonly rely on an assumed AAE_{BC}, which may introduce uncertainty into the separation of BC and BrC absorption because the spectral dependence of BC absorption can vary with its microphysical properties, including particle size, morphology, and coating characteristics (Luo et al., 2024; Luo et al., 2021; Zhang et al., 2020b). Nevertheless, this uncertainty is expected to primarily affect the quantitative partitioning of BC and BrC absorption, while the major spatial distribution and transport patterns of carbonaceous aerosols identified in this study are likely to remain robust.

https://doi.org/10.5194/egusphere-2026-4438
Preprint. Discussion started: 14 September 2026

Data availability

The HYSPLIT model, developed by the NOAA Air Resources Laboratory, is accessible via its official website at https://www.ready.noaa.gov/HYsPLIT.php. The meteorological data used in the HYSPLIT model were from the GDAS (ftp://arlftp.arlhq.noaa.gov/pub/archives/gdas1/), and the CALIPSO data obtained from the NASA Langley Research Center Atmospheric Science Data Center (https://asdc.larc.nasa.gov/), the MODIS AOD time-averaged map was generated using the GIOVANNI online data system (https://giovanni.gsfc.nasa.gov/giovanni/), and the fire data were from the Fire Information for Resource Management System (FIRMS, https://firms.modaps.eosdis.nasa.gov/).

Author contributions

Ju-Lian Shi: Conceptualization, Methodology, Formal analysis, Writing-original draft.
Chong-Shu Zhu: Conceptualization, Resources, Writing-review &editing.
Yao Qu: Investigation, Conceptualization, Data Curation, Validation.
Xiao Wang: Conceptualization, Data Curation, Formal analysis.
Nan Wang: Investigation, Data Curation.
Lu-Yao Wang: Investigation, Data Curation.
Wen-Ting Dai: Formal analysis, Conceptualization.
Hong Huang: Formal analysis, Conceptualization.
Jun-Ji Cao: Formal analysis, Conceptualization.

Competing interests

The authors declare that they have no conflict of interest.

Acknowledgments

This research was funded by the National Natural Science Foundation of China (42277098, 41771518), the Second Tibetan Plateau Scientific Expedition and Research

https://doi.org/10.5194/egusphere-2026-4438
Preprint. Discussion started: 14 September 2026

Program (STEP), Grant 2019QZKK0602, the Natural Science Basic Research Program of Shaanxi (Program No.2025JC-YBQN-430), and the Young Talent Fund of Xi'an Association for Science and Technology (0959202513117). The authors thank NASA for providing CALIPSO data and the MODIS AOD time-averaged map. The authors thank the NOAA Air Resources Laboratory for the HYSPLIT model and the NCEP for the GDAS meteorological data. The authors thank FIRMS for the fire counts data. We also appreciate the anonymous reviewers for their valuable comments.

Financial support

This research was funded by the National Natural Science Foundation of China (42277098, 41771518), the Second Tibetan Plateau Scientific Expedition and Research Program (STEP), Grant 2019QZKK0602, the Natural Science Basic Research Program of Shaanxi (Program No.2025JC-YBQN-430), and the Young Talent Fund of Xi'an Association for Science and Technology (0959202513117).

References

Andreae, M.O., Gelencer., A., 2006. Black carbon or brown carbon? The nature of light-absorbing carbonaceous aerosols. Atmos. Chem. Phys. 6, 3131-3148.

Bahadur, R., Praveen, P.S., Xu, Y., Ramanathan, V.J.P.o.t.N.A.o.S., 2012. Solar absorption by elemental and brown carbon determined from spectral observations. Proceedings of the National Academy of Sciences 109, 17366-17371.

Bonasoni, P., Laj, P., Marinoni, A., Sprenger, M., Angelini, F., Arduini, J., Bonafè, U., Calzolari, F., Colombo, T., Decesari, S., Di Biagio, C., di Sarra, A.G., Evangelisti, F., Duchi, R., Facchini, M.C., Fuzzi, S., Gobbi, G.P., Maione, M., Panday, A., Roccato, F., Sellegri, K., Venzac, H., Verza, G.P., Villani, P., Vuillermoz, E., Cristofanelli, P., 2010. Atmospheric Brown Clouds in the Himalayas: first two years of continuous observations at the Nepal Climate Observatory-Pyramid (5079 m). Atmos. Chem. Phys. 10, 7515-7531.

Carslaw, K., Boucher, O., Spracklen, D., Mann, G., Rae, J., Woodward, S., Kulmala,

https://doi.org/10.5194/egusphere-2026-4438
Preprint. Discussion started: 14 September 2026

M., 2010. A review of natural aerosol interactions and feedbacks within the Earth system. Atmos. Chem. Phys. 10, 1701-1737.

Devaprasad, M., Rastogi, N., Satish, R., Patel, A., Dabhi, A., Shivam, A., Bhushan, R., Meena, R., 2024. Dual carbon isotope-based brown carbon aerosol characteristics at a high-altitude site in the northeastern Himalayas: Role of biomass burning. Sci. Total Environ. 912, 169451.

Draxler, R., Rolph, G., 2012. HYSPLIT (HYbrid Single-Particle Lagrangian Integrated Trajectory) model access via NOAA ARL READY Website.available at NOAA Air Resources Laboratory, Silver Spring, MD. http://ready.arl.noaa.gov/HYSPLIT.php.

Drinovec, L., Močnik, G., Zotter, P., Prévôt, Ruckstuhl, C., Coz, E., Rupakheti, M., Sciare, J., Müller, T., Wiedensohler, A., Hansen, A.D.A., 2015. The "dual-spot" Aethalometer: an improved measurement of aerosol black carbon with real-time loading compensation. Atmos. Meas. Tech. 8, 1965-1979.

Fierce, L., Onasch, T.B., Cappa, C.D., Mazzoleni, C., China, S., Bhandari, J., Davidovits, P., Fischer, D.A., Helgestad, T., Lambe, A.T., Sedlacek, A.J., 3rd, Smith, G.D., Wolff, L., 2020. Radiative absorption enhancements by black carbon controlled by particle-to-particle heterogeneity in composition. Proc Natl Acad Sci U S A 117, 5196-5203.

Hindman, E.E., Upadhyay, B.P., 2002. Air pollution transport in the Himalayas of Nepal and Tibet during the 1995–1996 dry season. Atmos. Environ. 36, 727-739.

Huang, R.J., Li, Y.J., Chen, Q., Zhang, Y., Lin, C., Chan, C.K., Yu, J.Z., de Gouw, J., Tong, S., Jiang, J., Wang, W., Ding, X., Wang, X., Ge, M., Zhou, W., Worsnop, D., Boy, M., Bilde, M., Dusek, U., Carlton, A.G., Hoffmann, T., McNeill, V.F., Glasius, M., 2025. Secondary organic aerosol in urban China: A distinct chemical regime for air pollution studies. Science 389, eadq2840.

Huang, R.J., Yang, L., Cao, J., Chen, Y., Chen, Q., Li, Y., Duan, J., Zhu, C., Dai, W., Wang, K., Lin, C., Ni, H., Corbin, J.C., Wu, Y., Zhang, R., Tie, X., Hoffmann, T., O'Dowd, C., Dusek, U., 2018. Brown Carbon Aerosol in Urban Xi'an, Northwest

https://doi.org/10.5194/egusphere-2026-4438
Preprint. Discussion started: 14 September 2026

China: The Composition and Light Absorption Properties. Environ. Sci. Technol. 52, 6825-6833.

Hunt, W.H., Winker, D.M., Vaughan, M.A., Powell, K.A., Lucker, P.L., Weimer, C., 2009. CALIPSO lidar description and performance assessment. Journal of Atmospheric Oceanic Technology 26, 1214-1228.

IPCC, 2013. in: Stocker, T.F., Qin, D., Plattner, G.-K., Alexander, L.V., Allen, S.K., Bindoff, N.L., Bron, F.-M., Church, J.A., Cubasch, U., Emori, S. (Eds.), Summary for Policymakers, in:Climate change 2013: the physical science basis. Contribution of Working Group I to the Fifth Assessment Report of the Intergovernmental Panel on Climate Change. Cambridge University Press, pp. 129–234.

Kirchstetter, TW, Thatcher, TL, 2012. Contribution of organic carbon to wood smoke particulate matter absorption of solar radiation. Atmos. Chem. Phys. 2012,12(14), 6067-6072.

Kirchstetter, T.W., Novakov, T., Hobbs, P.V., 2004. Evidence that the spectral dependence of light absorption by aerosols is affected by organic carbon. J. Geophys. Res.: Atmos. 109.

Kirillova, E.N., Andersson, A., Tiwari, S., Srivastava, A.K., Bisht, D.S., Gustafsson, Ö., 2014. Water-soluble organic carbon aerosols during a full New Delhi winter: Isotope-based source apportionment and optical properties. J. Geophys. Res.: Atmos. 119, 3476-3485.

Kopacz, M., Mauzerall, D.L., Wang, J., Leibensperger, E., Henze, D.K., Singh, K., 2011. Origin and radiative forcing of black carbon transported to the Himalayas and Tibetan Plateau. Atmos. Chem. Phys. 11, 2837-2852.

Kumar, R., Naja, M., Satheesh, S.K., Ojha, N., Joshi, H., Sarangi, T., Pant, P., Dumka, U.C., Hegde, P., Venkataramani, S., 2011. Influences of the springtime northern Indian biomass burning over the central Himalayas. J. Geophys. Res. 116.

Laskin, A., Laskin, J., Nizkorodov, S.A., 2015. Chemistry of Atmospheric Brown Carbon. Chem. Rev. 115, 4335.

https://doi.org/10.5194/egusphere-2026-4438
Preprint. Discussion started: 14 September 2026

582 Laskin, A., West, C.P., Hettiyadura, A.P.S., 2025. Molecular insights into the
583 composition, sources, and aging of atmospheric brown carbon. Chem. Soc. Rev.
584 54, 1583-1612.
585 Levinson, R., Akbari, H., Berdahl, P.J.S.E., 2010. Measuring solar reflectance? Part I:
586 Defining a metric that accurately predicts solar heat gain. 84, 1717-1744.
587 Li, C., Bosch, C., Kang, S., Andersson, A., Chen, P., Zhang, Q., Cong, Z., Chen, B.,
588 Qin, D., Gustafsson, Ö., 2016. Sources of black carbon to the Himalayan-Tibetan
589 Plateau glaciers7. Nat. Commun. 7, 12574.
590 Li, X., Kang, S., Zhang, G., Qu, B., Tripathee, L., Paudyal, R., Jing, Z., Zhang, Y., Yan,
591 F., Li, G., 2018. Light-absorbing impurities in a southern Tibetan Plateau glacier:
592 Variations and potential impact on snow albedo and radiative forcing. Atmos. Res.
593 200, 77-87.
594 Liu, Z., Liu, D., Huang, J., Vaughan, M., Uno, I., Sugimoto, N., Kittaka, C., Trepte, C.,
595 Wang, Z., Hostetler, C., 2008. Airborne dust distributions over the Tibetan Plateau
596 and surrounding areas derived from the first year of CALIPSO lidar observations.
597 Atmos. Chem. Phys. 8, 5045-5060.
598 Lu, Z., Streets, D.G., Winijkul, E., Yan, F., Chen, Y., Bond, T.C., Feng, Y., Dubey, M.K.,
599 Liu, S., Pinto, J.P., R, C.G., 2015. Light absorption properties and radiative effects
600 of primary organic aerosol emissions. Environmental science and technology 49,
601 4868-4877.
602 Luo, J., Li, D., Wang, Y., Sun, D., Hou, W., Ren, J., Wu, H., Zhou, P., Qiu, J., 2024.
603 Quantifying the effects of the microphysical properties of black carbon on the
604 determination of brown carbon using measurements at multiple wavelengths.
605 Atmos. Chem. Phys. 24, 427-448.
606 Luo, J., Zhang, Y., Zhang, Q., 2021. Effects of black carbon morphology on brown
607 carbon absorption estimation: from numerical aspects. Geosci. Model Dev. 14,
608 2113-2126.
609 Nguyen, T.B., Lee, P.B., Updyke, K.M., Bones, D.L., Laskin, J., Laskin, A., Nizkorodov,
610 S.A., 2012. Formation of nitrogen- and sulfur-containing light-absorbing
611 compounds accelerated by evaporation of water from secondary organic aerosols.

https://doi.org/10.5194/egusphere-2026-4438
Preprint. Discussion started: 14 September 2026

J. Geophys. Res.

Pang, H., Zhang, Q., Lu, X., Li, K., Chen, H., Chen, J., Yang, X., Ma, Y., Ma, J., Huang, C., 2019. Nitrite-Mediated Photooxidation of Vanillin in the Atmospheric Aqueous Phase. Environ. Sci. Technol. 53, 14253-14263.

Qian, Y., Flanner, M.G., Leung, L.R., Wang, W., 2011. Sensitivity studies on the impacts of Tibetan Plateau snowpack pollution on the Asian hydrological cycle and monsoon climate. Atmos. Chem. Phys. 11, 1929-1948.

Qu, B., Ming, J., Kang, S.C., Zhang, G.S., Li, Y.W., Li, C.D., Zhao, S.Y., Ji, Z.M., Cao, J.J., 2014. The decreasing albedo of Zhadang glacier on western Nyainqentanglha and the role of light-absorbing impurities. Atmos. Chem. Phys. Discuss. 14.

Qu, Y., Liu, H., Zhou, Y., Zhang, Y., Shi, Y., Shi, J., Wang, N., Zhu, C., 2022. Optical properties and radiative forcing contribution of brown carbon in Xi'an during winter. China Environ. Sci. 42, 4486-4493.

Ramachandran, S., Rupakheti, M., Lawrence, M.G., 2020. Black carbon dominates the aerosol absorption over the Indo-Gangetic Plain and the Himalayan foothills. Environ. Int. 142, 105814.

Rovira, J., Yus-Díez, J., Chen, G.I., Močnik, G., Gysel-Beer, M., Aas, W., Aurela, M., Backman, J., Banerji, S., Brem, B.T., Canals-Angerri, A., Chazeau, B., Daellenbach, K.R., de Brito, J.F., Diapouli, E., Eleftheriadis, K., Ehn, M., Favez, O., Flentje, H., Gini, M.I., Granakis, K., Gregorič, A., Harrison, R., Heikkinen, L., Hueglin, C., Hyvärinen, A., Ivančič, M., Keernik, H., Liakakou, E., Lin, C., Lhotka, R., Luoma, K., Maasikmets, M., Manninen, H.E., Manousakas, M.I., Marchand, N., Mbengue, S., Mihalopoulos, N., Minguillón, M.C., Nicolae, D., Niemi, J.V., Ovadnevaite, J., Pérez, N., Petit, J.-E., Platt, S.M., Pokorná, P., Prévôt, A.S.H., Riffault, V., Rigler, M., Rinaldi, M., Schwarz, J., Stavroulas, I., Teinemaa, E., Teinilä, K., Timonen, H., Tobler, A., Vasilescu, J., Via, M., Vodička, P., Vratolis, S., Yttri, K.E., Zíková, N., Zografou, O., Alastuey, A., Petäjä, T., Querol, X., Pandolfi, M., 2026. Constraining the intensive absorption properties of ambient

https://doi.org/10.5194/egusphere-2026-4438
Preprint. Discussion started: 14 September 2026

organic aerosol particles based on pan-European observations. npj Clim. Atmos. Sci.

Saleh, R., Robinson, E.S., Tkacik, D.S., Ahern, A.T., Liu, S., Aiken, A.C., Sullivan, R.C., Presto, A.A., Dubey, M.K., Yokelson, R.J., 2014. Brownness of organics in aerosols from biomass burning linked to their black carbon content. Nat. Geosci. 7, 647-650.

Sellegri, K., Laj, P., Venzac, H., Boulon, J., Picard, D., Villani, P., Bonasoni, P., Marinoni, A., Cristofanelli, P., Vuillermoz, E., 2010. Seasonal variations of aerosol size distributions based on long-term measurements at the high altitude Himalayan site of Nepal Climate Observatory-Pyramid (5079 m), Nepal. Atmos. Chem. Phys. 10, 10679-10690.

Srivastava, D., Favez, O., Perraudin, E., Villenave, E., Albinet, A., 2018. Comparison of measurement-based methodologies to apportion secondary organic carbon (SOC) in PM2. 5: a review of recent studies. Atmosphere 9, 452.

T. C. Bond, S. J. Doherty, D. W. Fahey, P. M. Forster, T. Berntsen, B. J. DeAngelo, M. G. Flanner, S. Ghan, B. Kärcher, D. Koch, S. Kinne, Y. Kondo, P. K. Quinn, M. C. Sarofim, M. G. Schultz, M. Schulz, C. Venkataraman, H. Zhang, S. Zhang, Bellouin, N., S. K. Guttikunda, P. K. Hopke, M. Z. Jacobson, J. W. Kaiser, Z. Klimont, U. Lohmann, J. P. Schwarz, D. Shindell, T. Storelvmo, S. G. Warren, Zender, C.S., 2013. Bounding the role of black carbon in the climate system: A scientific assessment Journal of Geophysical Research Atmospheres 118.

Wang, Q., Han, Y., Ye, J., Liu, S., Pongpiachan, S., Zhang, N., Han, Y., Tian, J., Wu, C., Long, X., 2019. High contribution of secondary brown carbon to aerosol light absorption in the southeastern margin of Tibetan Plateau. Geophys. Res. Lett. 46, 4962-4970.

Winker, D.M., Hunt, W.H., Mcgill, M.J.J.G.R.L., 2007. Initial performance assessment of CALIOP. Geophys. Res. Lett. 34, 228-262.

Winker, D.M., Vaughan, M.A., Omar, A., Hu, Y., Powell, K.A., Liu, Z., Hunt, W.H., Young, S.A., 2009. Overview of the CALIPSO mission and CALIOP data processing algorithms. Journal of Atmospheric Oceanic Technology 26, 2310-

https://doi.org/10.5194/egusphere-2026-4438
Preprint. Discussion started: 14 September 2026

2323.

Xu, J., Hettiyadura, A.P.S., Liu, Y., Zhang, X., Kang, S., Laskin, A., 2020. Regional Differences of Chemical Composition and Optical Properties of Aerosols in the Tibetan Plateau. J. Geophys. Res.: Atmos. 125.

Yang, Y., Zhao, C., Wang, Q., Cong, Z., Yang, X., Fan, H., 2021. Aerosol characteristics at the three poles of the Earth as characterized by Cloud–Aerosol Lidar and Infrared Pathfinder Satellite Observations. Atmos. Chem. Phys. 21, 4849-4868.

Yu, Z., Tian, P., Kang, C., Song, X., Huang, J., Guo, Y., Shi, J., Tang, C., Zhang, H., Zhang, Z., Cao, X., Liang, J., Zhang, L., 2024. Physical Properties, Chemical Components, and Transport Mechanisms of Atmospheric Aerosols Over a Remote Area on the South Slope of the Tibetan Plateau. J. Geophys. Res.: Atmos. 129.

Zhang, M., Zhao, C., Cong, Z., Du, Q., Xu, M., Chen, Y., Chen, M., Li, R., Fu, Y., Zhong, L., Kang, S., Zhao, D., Yang, Y., 2020a. Impact of topography on black carbon transport to the southern Tibetan Plateau during the pre-monsoon season and its climatic implication. Atmos. Chem. Phys. 20, 5923-5943.

Zhang, X., Mao, M., Yin, Y., Tang, S., 2020b. The absorption Ångstrom exponent of black carbon with brown coatings: effects of aerosol microphysics and parameterization. Atmos. Chem. Phys. 20, 9701-9711.

Zhang, Z., Wang, Y., Chen, X., Xu, L., Zheng, Z., Ching, J., Zhu, S., Liu, D., Li, W., 2025. Absorption enhancement and shielding effect of brown organic coating on black carbon aerosols. npj Clim. Atmos. Sci. 8.

Zhu, C.S., Cao, J.J., Hu, T.F., Shen, Z.X., Tie, X.X., Huang, H., Wang, Q.Y., Huang, R.J., Zhao, Z.Z., Mocnik, G., Hansen, A.D.A., 2017. Spectral dependence of aerosol light absorption at an urban and a remote site over the Tibetan Plateau. Sci. Total Environ. 590-591, 14-21.

Zhu, C.S., Qu, Y., Dai, W.T., Su, X.L., Zhou, J.M., Wang, N., Qu, J., Cao, J.J., 2022a. Comparison of black carbon, primary and secondary brown carbon light absorption and direct solar absorption at the foothill and summit of Mt. Hua, China. Sci. Total Environ. 848, 157814.

https://doi.org/10.5194/egusphere-2026-4438
Preprint. Discussion started: 14 September 2026

699 Zhu, C.S., Qu, Y., Huang, H., Chen, J., Dai, W.T., Huang, R.J., Cao, J.J., 2021. Black
700 Carbon and Secondary Brown Carbon, the Dominant Light Absorption and Direct
701 Radiative Forcing Contributors of the Atmospheric Aerosols Over the Tibetan
702 Plateau. Geophys. Res. Lett. 48.
703 Zhu, C.S., Qu, Y., Huang, H., Shi, J.L., Dai, W.T., Zhang, N.N., Wang, N., Wang, L.Y.,
704 Ji, S.S., Cao, J.J., 2024. Brown Carbon From Biomass Burning Reinforces the
705 Himalayas and Tibetan Plateau Warming. Geophys. Res. Lett. 51.
706 Zhu, C.S., Qu, Y., Zhang, Z.S., Zhang, T., Dai, W.T., Cao, J.J., 2022b. High Spatial
707 Variability of Biomass Burning Emissions Observed at Three Tibetan Plateau Sites.
708 Earth's Future 10.
709